Functionally Graded Materials designed for thrusters : resistance under laser thermal flux and in combustion environment

Lisa Audouard, Aurélie Julian-Jankowiak, Jean-François Justin, Pierre Bertrand, Cécile Langlade, Matthieu Garcia, Lucien Vingert

DOI: 10.13009/EUCASS2023-295
Aerospace Europe Conference 2023 – 10TH EUCASS – 9TH CEAS

Functionally Graded Materials designed for thrusters : resistance under laser thermal flux and in combustion environment

Lisa AUDOUARD [123]*, *Aurélie JULIAN-JANKOWIAK* [1], *Jean-François JUSTIN* [1], *Pierre BERTRAND* [2], *Cécile LANGLADE* [2], *Matthieu GARCIA* [3], *Lucien VINGERT* [4]
[1] *ONERA/DMAS-Université de Paris-Saclay, 92320, Châtillon, France*
(lisa.audouard@onera.fr; aurelie.jankowiak@onera.fr, jean-francois.justin@onera.fr)
[2] *Université de Bourgogne Franche-Comté, laboratoire ICB UMR CNRS-UB-UTBM 6303, 90010 Belfort France*
(cecile.langlade@utbm.fr; pierre.bertrand@utbm.fr)
[3] *Direction des systèmes orbitaux, CNES, Toulouse, 31410, France* (Matthieu.Garcia@cnes.fr)
[4] *ONERA/DMPE-Université de Paris-Saclay, 91120, Palaiseau, France* (lucien.vingert@onera.fr)
* *Corresponding author*

Abstract
Functionally Graded Materials (FGM) are developed by ONERA, CNES and ICB to withstand harsh thermal and environmental conditions induced by new green propellants in satellite thrusters. In this study, different types of FGM are elaborated through Atmospheric Plasma Spraying (APS) and tested in representative environments to assess the influence of the FGM composition profile. In particular, the resistance of FGM facing thermal shock tests is evaluated with a laser test bench, and its resistance in oxidative flow in a combustion chamber with a H_2/O_2 flame. FGM with thin ceramic layer exhibit very good behavior under these conditions.

1. Introduction

Low Earth Orbit satellites are equipped with low-thrusts engines (about 1 N) to correct their orbital position and orientation, which are disturbed by both atmosphere and gravitation effects. These thrusters often use anhydrous hydrazine due to its high efficiency and reliability. However, as hydrazine is a very toxic propellant, its use is threatened by European regulations [1]. Thus, studies about the development of alternative efficient and less toxic propellants emerged [2–4]. In this context, CNES has developed a “green” monopropellant to replace hydrazine but it induces harsher operating conditions for the materials of the combustion chamber, in terms of temperature and oxidation. In particular, the temperature flame reaches 2700 K during firing and the associated atmosphere is notably constituted of water vapor, which is a very oxidative compound. In addition, the material system used in the thrusters must endure several short duration firings, which are responsible for thermal shock of the materials. Consequently, the material system used with hydrazine is not resilient enough considering the harsh environment of these new green monopropellants.
Thus, ONERA, CNES and ICB have engaged a close collaboration to develop materials able to withstand these new requirements. Among all, ceramic/metal Functionally Graded Materials (FGM) seem to be very promising. Ceramic/metal FGM are constituted of a ceramic top layer exposed to the flame acting as a thermal and environmental barrier coating, several cermet graded layers and a refractory metal underneath [5–7]. The interest of such a material system is to limit the stress concentrations at the interfaces of classic ceramic/metal bilayer systems. Indeed, the coefficient of thermal expansion of the ceramic and the metal may be highly different as well as sintering behavior and mechanical properties. During firings of the thruster, the stresses increase between the two materials and finally lead to deleterious damages, such as complete spallation of the ceramic part, which induce catastrophic failures in the bilayer systems. Contrariwise, FGM can prevent or at least considerably delayed these phenomena as they reduce stresses with graded cermet layers between pure ceramic and pure metal layer [8,9]. Several authors have studied the performances of FGM under harsh thermal and environmental conditions, but the investigated temperatures are often limited to 1400 K [10]. Indeed, the main studied applications for FGM are in the field of engines for aeronautics, for which the operating temperatures are lower compared to satellite propulsion, but the time exposures are longer. In this context, the oxidation behavior and thermal shock resistance of M-CrAl(Y/Zr)/YSZ FGM dedicated to the aeronautical field have been investigated by many authors [11–16]. Some studies present the resistance of FGM submitted to a combustion test with an H_2/O_2 flame. For example, Kawasaki and Watanabe brought out the chronology of successive phenomena leading to final failure in an YSZ/stainless steel FGM [10]. More precisely, during heating, non-linear deformation occurs due to compressive stress yields. After that, during cooling, residual tensile stresses appear which are responsible for vertical cracking. These cracks are deflected, propagate parallel to the surface and finally lead to crack coalescence and spalling [10]. The same authors also investigated the performance of different conceptions of

DOI: 10.13009/EUCASS2023-295

YSZ/NiCrAlY FGM manufactured through plasma spraying under consecutive thermal shocks generated by a combustion flame [5]. It was found that the composition profile of the FGM determined the number of cycles to spall. More specifically, linear graded FGM allow to multiply by 10 the number of cycles to spall compared to a non-linear composition profile for a temperature gradient of 400 K in the YSZ layer. Thus, even if some data exist about the resistance of FGM under harsh conditions, the temperature and the thermal shock considered in these studies are much lower compared to the present application. Only one study deals with the resistance of a FGM under near real space combustion chamber environment up to 2300 K [17]. The SiC/C FGM system evaluated in this study undergoes 2 firing cycles of 55 s duration each without presenting damage. Thus, experiments and knowledge concerning the resistance of ceramic/metal FGM at high temperatures in near real environment are missing.
The present study was conducted in this context and aims to develop and characterise a ceramic/metal FGM able to endure near real satellite combustion chamber conditions. Thus, four composition profiles of FGM were elaborated using Atmospheric Plasma Spraying (APS) and were tested on two test benches able to reproduce operating temperatures. More specifically, the resistance of the different FGM was firstly evaluated with a CO_2 laser test bench under vacuum and secondly in a combustion chamber with a H_2/O_2 flame. The composition profiles vary with the chemical composition of the ceramic, the thickness of the pure ceramic layer and the thickness of the graded cermet layers. In addition, variable tests conditions were studied on the two test benches in order to asset the link between the test conditions and the degradation phenomena.

2. Experimental procedure

2.1. Manufacturing of the FGM

This study aims to analyse the influence of the composition profile of the FGM in severe environment. Thus, four types of FGM are manufactured. More specifically, commercial ceramic and metal powders are used. For the ceramic part, yttria stabilised hafnia is chosen due to its high stability, thermal insulation and resistance to water vapor under ultra-high temperatures [18–20], which are determining criterion for the intended application. The four types of FGM differ in the nature of the ceramic (HfO_2 + 12 mol% of Y_2O_3 named 12YSHf or HfO_2 + 33 mol% of Y_2O_3 named 33YSHf), the thickness of the pure ceramic top layer (180 or 300 µm) and the thickness of the graded layers (500 or 700 µm). The four types of FGM are summarised in Figure 1(b). All the samples are elaborated by APS at ICB, which is equipped with a F4MB plasma torch. APS is a classical manufacturing process for applying coatings on combustion chamber materials. This is due in particular to its ability to be industrialised and to manufacture complex shapes quite rapidly. This process, presented in Figure 1(a), was also used for the manufacturing of FGM in other studies [6,21].

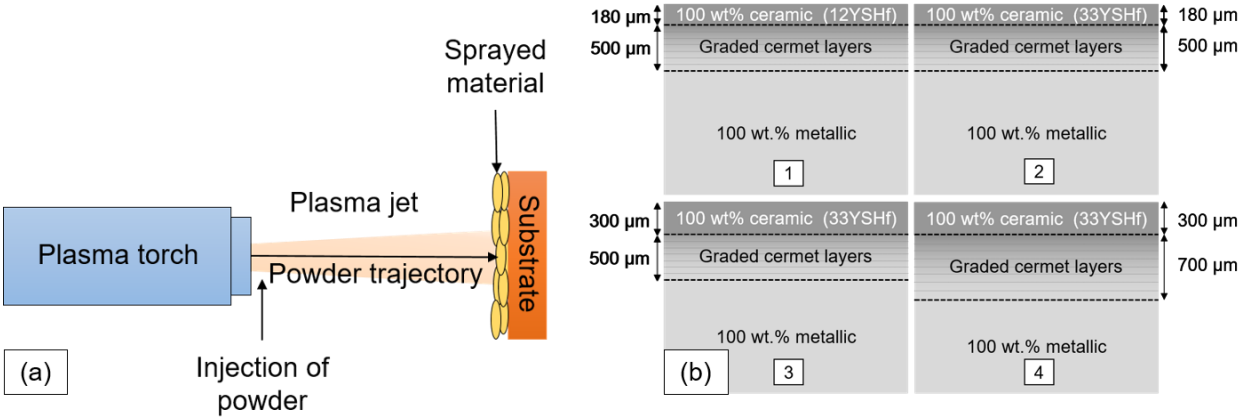

Figure 1: Schematic representation of (a) the APS process and (b) the four studied FGM configurations.

Before the elaboration, ceramic/metal mixtures intended to be used for the graded cermet layers of the FGM are prepared following a granulation process. Then, the 2 mm thick FGM are build layer by layer on a specific substrate. The spraying parameters are adjusted depending on the composition of the sprayed powders to provide optimised deposit efficiency and appropriate heat transfer. The composition profile of the FGM is expected to follow a power law type.
As the spraying of the FGM is performed under air, metallic oxides are formed in the plasma and are constitutive part of the final material. These metallic oxides are detrimental to the mechanical resistance, thus they need to be eliminated before the resistance tests. For this reason, FGM are submitted to a 1 h thermal treatment at 1423 K under vacuum,

DOI: 10.13009/EUCASS2023-295

which allows the oxides vaporization. Moreover, as the porosity level after APS is close to 12 %, which is relatively high, a final thermal treatment of densification is lead at 2273 K during 1 h under Ar.

2.2. Vacuum laser test bench

Considering the intended application, the resistance to thermal shock with high temperature differences must be determined. The Onera's CO_2 laser test bench (3 kW, 10.6 µm) allows to reach ultra-high temperatures under different atmospheres. In order to isolate the degradation mechanisms related to the temperature from the ones associated to the oxidising environment, the tests are performed under vacuum (10^{-2} mbar). On this bench, the laser flux is perpendicular to the surface of the tested sample. The temperature is monitored by a power input. In addition, a bichromatic pyrometer is set up to control the surface temperature of the sample. For all the tests, a 200 K s^{-1} heating rate assures thermal shock conditions. The varying test parameters are the upper surface temperature (between 2053 and 2623 K), the number of cycles (1 or 25 cycles) and the duration of the cycles (60 or 3600 s). A typical example of a 25 cycles thermal shock test is presented in Figure 2(a). The FGM samples used for these tests are squares with dimensions 15 mm x 15 mm (2 mm thick). The size of the laser spot is chosen to include the whole sample in the laser flux, which is homogeneous as a top hat beam shaper is used in the optical way. The dimension and shape of the laser spot is presented in Figure 2(b).

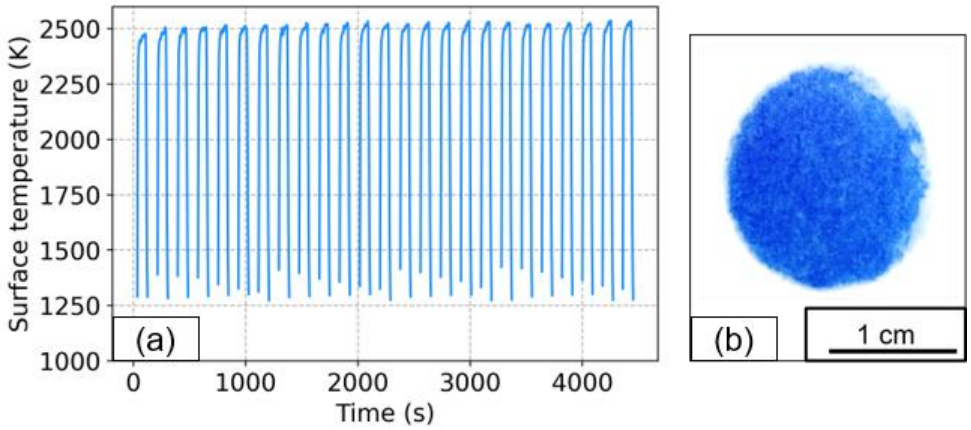

Figure 2: (a) Representation of a thermal shock test constituted of 25 short cycles of 60 s at 2523 K and (b) visualisation of the size and shape of the laser spot.

Thus, in this study, the laser test bench is dedicated to the determination of the FGM resistance to thermal shock under vacuum. As the surface temperature is measured with a pyrometer, the link between the observed phenomena and the temperature can be achieved. Moreover, the test possibilities are numerous and relatively free. However, considering the intended application, the behavior of the materials must also be determined in an oxidising atmosphere.

2.3. Combustion chamber test bench

To determine the behavior and the resistance of the FGM under near real environmental conditions, the combustion test bench MASCOTTE is used (Figure 3(a)). More precisely, in this facility, an H_2/O_2 flame is generated in the combustion chamber, approaching real satellite thruster flame. At a given chamber pressure, the flame temperature only depends on the mixture ratio. Thus, the flow rates of H_2 and O_2 are chosen to reach a 3200 K flame temperature and checked by calculation after each test to ensure the accordance between previsions and experimental data. To be consistent with the targeted application, the pressure is set at 10 bar for all the tests. During the test, the surface temperature of the FGM is not known with precision, at the difference of the laser tests, as it is difficult to set up instrumentation in this facility. Despite this, two thermocouples (S type) were introduced in the rear face of the sample, thus measuring a much lower temperature compared to the real surface temperature. Indeed, for a 3200 K flame temperature, the thermocouples only indicate 1500 K (Figure 3(c)).
Four tests have been conducted on this bench and are described in Table 1. For each test, all FGM types are assessed simultaneously to be able to compare the influence of FGM type on their resistance in the combustion chamber. All of the tests reach a 3200 K flame temperature under a pressure of 10 bar but differ one from the other with the cumulative time exposure. Indeed, the FGM are exposed in the flame from 2 to 10 cycles of 150 s each. They are introduced in the sample holder, specifically designed for this experimental campaign (Figure 3(b)), allowing the FGM to be in the flow during firings but not at the stagnation point. The different steps of a hot run are presented in Figure 3(c). The

DOI: 10.13009/EUCASS2023-295

combustion products generated by an H_2/O_2 flame at 3200 K are 87 wt% of H_2O, 6.5 wt% of H_2 and 5 wt% of $\cdot OH$. Thus, for the tested FGM, these products are responsible for a very severe oxidizing environment.

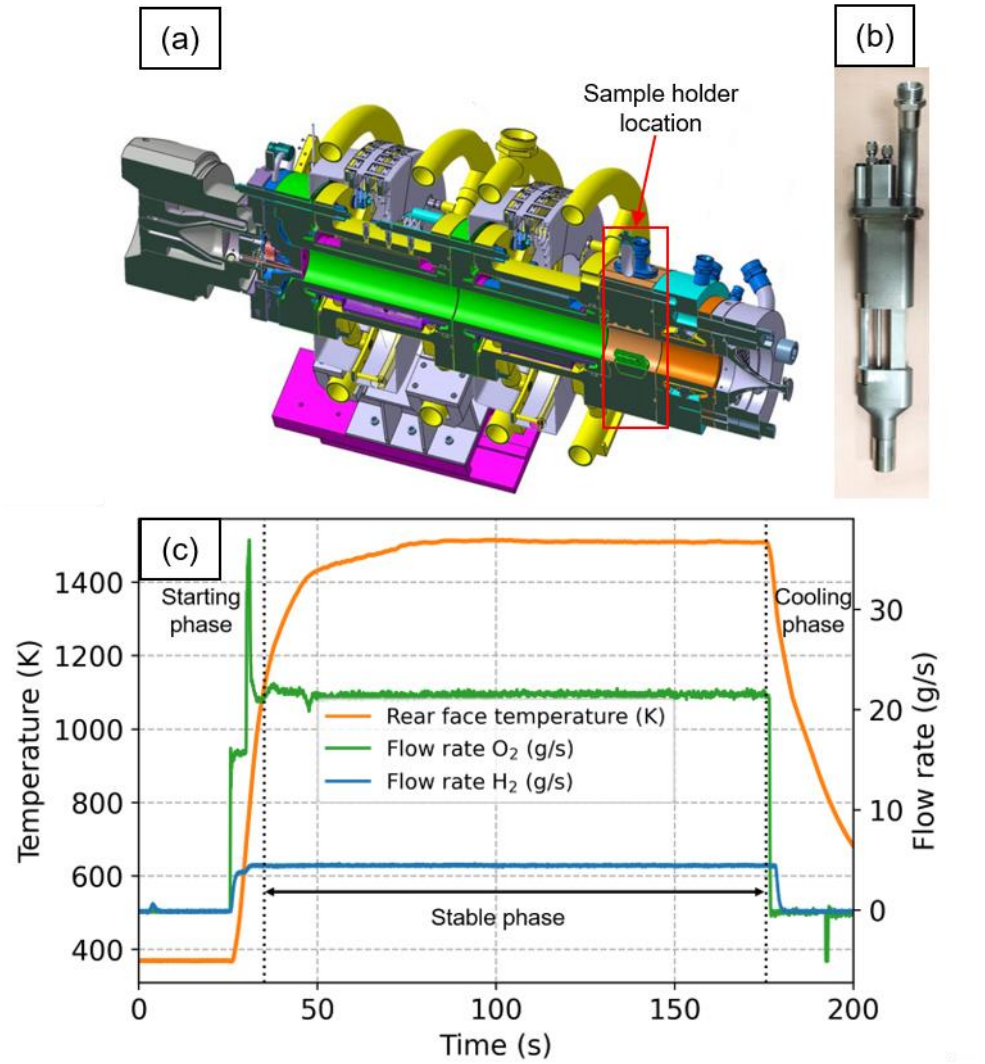

Figure 3: (a) Schematic representation of the combustion chamber with the sample holder location, (b) photograph of the sample holder without FGM installed and (c) presentation of the different steps of a hot run.

Table 1: Tests conditions in the MASCOTTE Facility.

Test number	Flame temperature (K)	Period of hot runs
I	1200, 1500, 2000, 2500, 3000, 3200	25 s x 5 + 75 s
II	3200	85 s + 150 s
III		150 s x 4
IV		150 s x 10

2.4. Sample characterisations

The aspect, the microstructure and the composition of the top surface of all the samples are investigated before and after the different tests. More specifically the crack networks generated by the final high temperature thermal treatment

DOI: 10.13009/EUCASS2023-295

are identified with an optical microscope and a Scanning Electron Microscope (Tescan Mira3 Schottky FEG-SEM). In addition, the phase composition is investigated before and after the tests by X-ray diffraction (XRD) technique using an Empyrean PANalytical device in Bragg-Brentano configuration (θ–θ and Cu Kα radiation). After surface analyses, cross-section investigations are conducted through optical and SEM microscopes and Energy Dispersive Spectroscopy analyses (EDS) using an EDAX Octan Elite EDS system. For that, samples are embedded in an epoxy resin, longitudinally cut and mechanically grinded with SiC papers and polished with diamond suspensions down to 0.25 µm.

3. Results and discussion

3.1. Microstructural and chemical characterisation of as sprayed and thermal treated FGM

The cross-section microstructure of all FGM types is investigated after APS elaboration to ensure the homogeneity of the deposit as well as to constitute a reference to be compared with microstructures after the thermal treatment at 2273 K and after the laser and combustion tests. Examples of the cross-section of a type-3 FGM after APS and thermal treatment are given in Figure 4. The ceramic part corresponds to the darker phase whereas the metal part corresponds to the lighter phase. Observable black areas are due to porosities or unmelted particles. The microstructure is lamellar, which is a characteristic after APS elaboration. Also, the layers seem to be well bonded and no delamination is observable neither before nor after the thermal treatment. It is observable that the thermal treatment at 2273 K allows to reach a much higher densification rate of the ceramic part compared to before the thermal treatment. However, this thermal treatment is responsible for the creation of a crack network in the pure ceramic top layer. This crack formation may be explained by two competing phenomena. First, the sintering of the ceramic is different from the sintering of the metal, which is demonstrated by the difference in the densification rate observed in Figure 4(b). Moreover, the thermal expansion mismatch between the ceramic and the metal may be responsible for the formation of cracks in the ceramic part during the cooling stage of the thermal treatment.

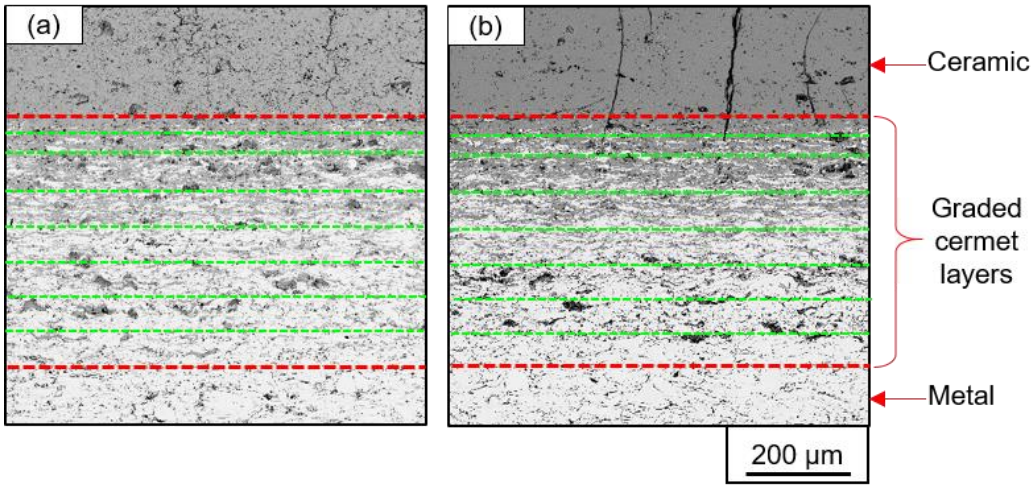

Figure 4: SEM (BSE) observation of the cross-section of a type-3 FGM sample (a) after elaboration through APS and (b) after elaboration through APS and thermal treatment at 2273 K.

Also, XRD analyses carried out on the surface of FGM after APS elaboration reveal that only the fluorite $Y_2Hf_2O_7$ phase is detected for FGM with 33YSHf as a ceramic and a cubic yttria-enriched HfO_2 phase is detected for FGM with 12YSHf as a ceramic. This is under expectation as the ideal amount of Y_2O_3 in HfO_2 to form $Y_2Hf_2O_7$ is 33 mol% [22]. This demonstrates that the expected phases are effectively formed during the elaboration process, as the initial ceramic powders are only constituted of a mixture of Y_2O_3 and HfO_2 without synthesis step. However, after the thermal treatment, HfC is also detected on the surface of some FGM. The presence of HfC may be due to the graphite susceptors in the furnace used for the thermal treatment under inert atmosphere.

3.2. Resistance of the FGM under laser thermal flux in vacuum

The resistance of types-1,2,3 FGM is tested under laser thermal flux in vacuum. After laser tests, none of the sample present visible signs of surface degradation. The surface of all FGM is investigated by SEM to visualise the crack network evolution. The micrographs of the same type-1 FGM before the laser test, after 1 cycle at 2473 K during 60 s and after 26 cycles at 2473 K during 60 s each are gathered in Figure 5. From this figure, it is observable that the crack

DOI: 10.13009/EUCASS2023-295

network before the test and after one cycle of 60 s at 2473 K is completely different. Indeed, the cracks related to the thermal treatment disappear from the surface of the FGM since they are not detectable on Figure 5(b). Instead of the initial crack network, a new crack network is established. The morphology of this new network is a little different from the previous one, as it seems to present more interconnected points between cracks. After 25 additional cycles at 2473 K during 60 s on the same FGM sample, the crack network, which has been formed during the first cycle is still detected and almost identical. Indeed, at the surface, there is no creation of new cracks and the crack network is stable cycle after cycle. The only difference is the crack opening, which is more pronounced after 26 cycles. This observation means that the first cycle determine the crack network and that the temperature seems to play a major role on crack formation compared to the number of cycles.

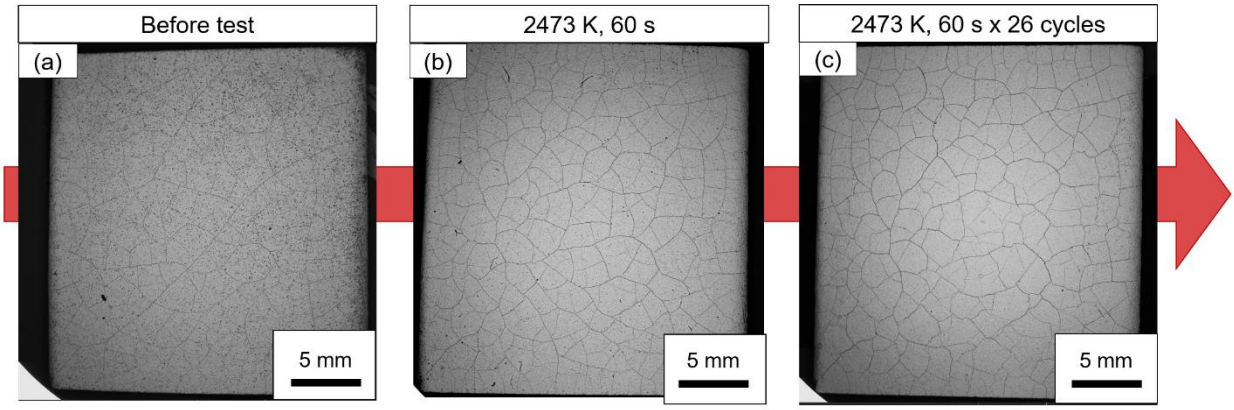

Figure 5 : SEM (BSE) surface observations of the same FGM sample (a) before the test, (b) after one laser test cycle of 60 s under vacuum at 2473 K and (c) after 26 cycles of 60 s under vacuum at 2473 K.

This modification of the crack network is observable on all FGM samples tested over 2143 K. Indeed, for the FGM sample tested at 2053 K, no evolution of the crack network is detectable between before and after the laser test. This means that the transient temperature above which the crack network evolution occurs, is included between 2053 K and 2143 K.

To try to explain the crack network evolution before and after the laser tests, XRD examinations are carried out on the FGM surfaces. These investigations provide a better understanding of the influence of vacuum laser thermal shock tests on the surface phases stability. The diagrams are recorded for 2Θ from 10 ° to 110 ° but to provide a better visualisation, the results are only presented from 45 ° to 65 °. Thus, four XRD surface diagrams of samples tested at different temperatures during one cycle of 60 s are reported in Figure 6(a). From this figure, the FGM tested at the lowest temperature (2053 K) is very crystalline and composed of only one phase, which is the fluorite $Y_2Hf_2O_7$ phase, already present before the test. Thus, at 2053 K during 60 s under vacuum, the fluorite phase is stable. However, increasing the test temperature leads to a phase destabilisation at the sample surface, which is visible on Figure 6. Indeed, after tests at 2143 K, 2413 K and 2623 K, the phases are less crystalline since the Full-Width Half Maximum (FWHM) of the peaks is much larger. This change in the peak shapes are related to a phase destabilisation, which becomes more pronounced with increasing test temperature.

The peaks identification on the FGM tested at 2143 K revealed that the peaks can be simulated by an yttria-rich phase which is $Y_{0.7}Hf_{0.3}O_{1.65}$ (space group Fm-3m), chemically close to the stoichiometric $Y_2Hf_2O_7$, but differing by the ratio between Y, Hf and O. In addition, a shoulder is detected on the left side of the peaks and can be simulated with pure Y_2O_3 (space group Ia-3). The calculated lattice parameters of the destabilised phases $Y_{0.7}Hf_{0.3}O_{1.65}$ and Y_2O_3 are respectively 5.2240 Å and 10.5616 Å. As the theoretical lattice parameter of Y_2O_3 is 10.6017 Å, it is probable that the Y_2O_3 phase is slightly doped in Hf. In particular, the $Y_{1.69}Hf_{0.31}O_{3.155}$ (space group Ia-3) phase also fits (but with less accuracy) the shoulder on the XRD diagram, which tends to show the presence of a slight quantity of Hf in Y_2O_3. However, this quantity could not be precisely quantified through surface XRD analysis of thermal sprayed FGM. Also, it can be seen from Figure 6(b) that the experimental and calculated profiles are very close.

DOI: 10.13009/EUCASS2023-295

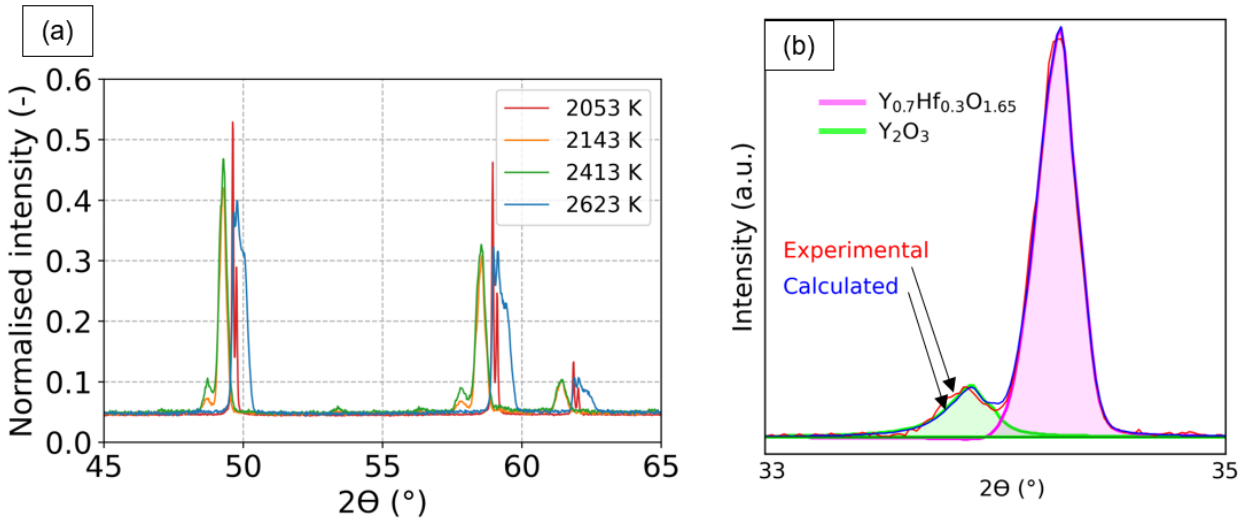

Figure 6: (a) XRD diagrams of the surface of FGM samples after laser tests under vacuum performed at 2053 K, 2143 K, 2413 K and 2623 K and (b) XRD diagram (zoom for 2Θ from 33 ° to 35 °) of an FGM sample after laser test at 2143 K during 60 s and corresponding phase simulation.

To better understand the destabilisation process, SEM examinations coupled with EDS analyses are carried out on FGM cross-sections after the tests, and in particular in the 125 µm under the surface. An EDS profile along these 125 µm reveals that phase destabilisation is detectable by EDS analyses down to about 50 µm below the surface and is more particularly intense just a few µm under the surface. SEM (BSE) cross section of this interest zone is presented in Figure 7(a). A strong chemical contrast is detectable in dark grey just under the surface and even under this zone, a chemical gradient is observable. The green arrow on the image corresponds to the EDS profile and the semi quantitative analyses of the weight proportions of the different elements is presented in Figure 7(b). Therefore, the dark layer with the strong chemical contrast corresponds to a rich yttria layer. Also, a gradient of yttria concentration is detectable under this layer. Observable variations between approximately 11 and 17 µm should not be taken into account as they correspond to the presence of a porosity crossing the EDS profile. Indeed, a porosity region is detected parallel to the surface where phase destabilisation occurs, from about 10 to 20 µm depth. This porosity was not detected before the test and seems to be related to chemical variations. Thus, phase destabilisation detected through XRD analyses corresponds to the segregation of yttrium and hafnium through diffusion phenomena. In particular, the dark layer seems to correspond to the Y_2O_3 phase (in green on Figure 6(b)), while the yttria graded composition underneath seems to be related to the $Y_{0.7}Hf_{0.3}O_{1.65}$ phase (in pink on Figure 6(b)).

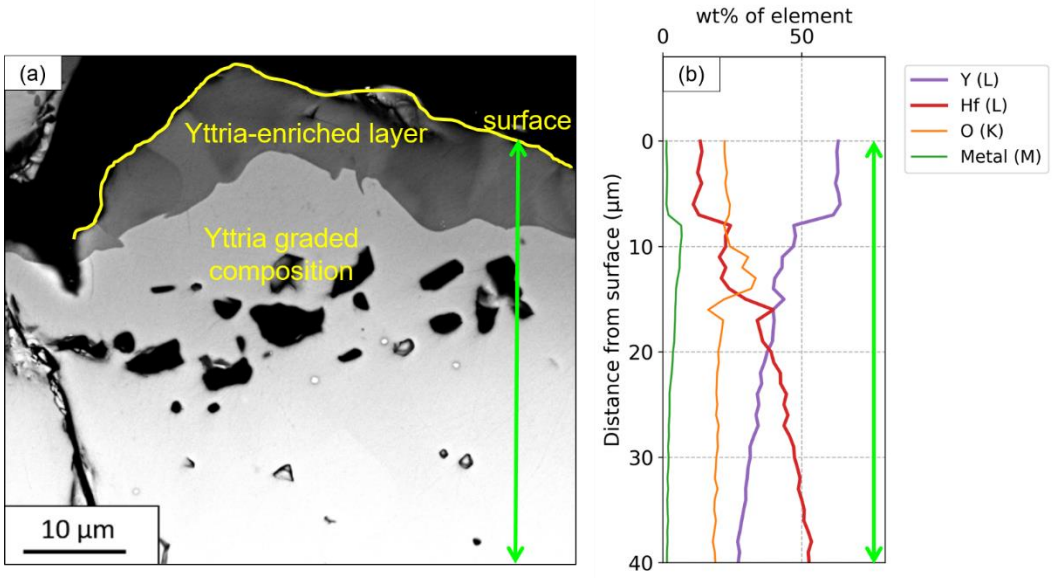

Figure 7 : (a) SEM (BSE) observation of the cross section of an FGM after laser test at 2143 K during 60 s and (b) corresponding chemical elements profile analyses (wt%) by EDS along the cross section (green arrows).

DOI: 10.13009/EUCASS2023-295

It has been observed by SEM analysis that the yttria-enriched layer is not continuous along the top surface and is relatively thin, which explains that the main phase detected through XRD analysis is the $Y_{0.7}Hf_{0.3}O_{1.65}$ and not Y_2O_3. EDS analysis confirms the presence of a slight quantity of Hf even at the top surface, despite the yttria enrichement is clearly high. Thus, XRD and EDS analysis are in good agreement. However, the destabilisation occuring at 2623 K is less clear but is currently under investigation. The presence of a porosity layer underneath the yttria-enriched layer is consistent with diffusion phenomena. Indeed, the diffusion rate of Y^{3+} in $Y_2Hf_2O_7$ may be different from the diffusion rate of Hf^{4+} in $Y_2Hf_2O_7$. This difference can finally lead to the creation of holes in the material. This effect, known as the Kirkendall effect, has already been observed for yttria stabilised hafnia ceramics [23] but also for other materials in the literature [24–26].
It has to be noticed that chemical destabilisation is far more pronounced for FGM containing 33YSHf as a ceramic (types-2,3,4) than for FGM with 12YSHf (type-1). This is probably correlated to the fact that higher amount of yttria in hafnia leads to higher differences in the diffusion rates compared to lower amount.
Bringing together the experimental SEM examinations, EDS and XRD analyses, the link between the evolution of the crack network and the change in the chemical composition at the surface of the FGM can be established. Indeed, after a cycle of 60 s at 2053 K, the surface composition is constituted of a very crystalline phase with no destabilisation and the crack network is identical to the one before the test. For all the other tested temperatures, the crack network is modified and the surface presents destabilised phases associated to an yttria gradient in depth (about 50 µm). Thus, during the laser test, there is a diffusion of yttrium and hafnium ions, which is responsible for a chemical gradient at the FGM surface and for phase destabilisation. To explain the crack network evolution, two hypotheses may be proposed. These two assumptions are based on the supposition that the destabilised phases formed may be less refractory than the initial $Y_2Hf_2O_7$. The first one is that this can lead to partial melting at the surface, which may repair the cracks during heating. During cooling, a new crack network is created and phase heterogeneities are fixed since FGM is submitted to a thermal shock (200 K s^{-1}). The second hypothesis is that sintering occurs in these destabilised phases above 2053 K even if test durations are very short (60 s). Sintering may close the initial cracks and new cracks appear during the cooling phase of the laser test. The first hypothesis would suggest that this process will be repeated at each cycle but that is not in accordance with our experimental observations. Thus, the second hypothesis is more probable and is strengthened by the fact that the size of the grains in the destabilised depth is much larger than the size of the grains under the destabilised depth (> 50 µm) as it visible in Figure 8. Indeed, grain growth occurs during the last stage of sintering. As the FGM on this figure has been tested during 3600 s, the grain size differences are particularly remarkable.

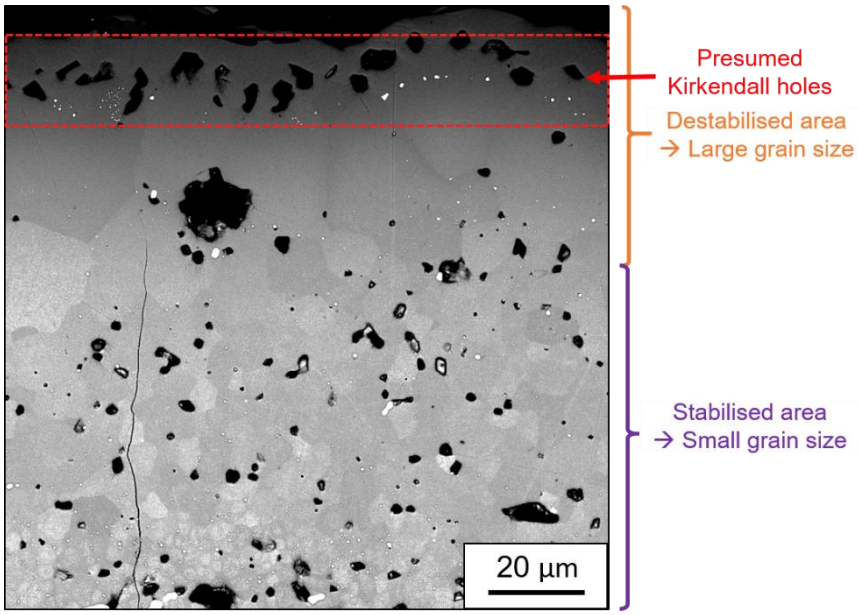

Figure 8 : SEM (BSE) cross-section observation of an FGM after one cycle of laser test at 2473 K during 3600 s allowing to visualise the presumed Kirkendall holes and the bimodal grain size distribution in depth.

Finally, none of the cross section microstructures of the FGM present any sign of total spallation. In addition, for the short tests (one cycle of 60 s) the crack network is limited to the ceramic or the rich ceramic graded layers, indicating that the FGM resist quite well in the tested conditions. However, for the FGM which has been cycled 26 times during 60 s at 2473 K, cracks are more opened and reach the metal rich graded layers (not shown here). Also, for the FGM

DOI: 10.13009/EUCASS2023-295

type-3 having the thickest ceramic top layer, the cracks are deeper and the distance between cracks is larger compared to FGM with the thinnest ceramic top layer (types-1 and 2).
Thus, laser tests brought many information on the resistance of FGM submitted to thermal shocks under vacuum. Firstly, the crack network is modified above 2143 K. This may be correlated to a surface chemical modification, linked to diffusion and sintering phenomena. Also, it has been established that the nature of the ceramic has a role on phase destabilisation. Indeed, FGM type-2 and 3 containing the higher amount of yttrium are submitted to more pronounced destabilisation than the FGM type-1. In addition, the thickness of the ceramic top layer influences the crack depth. Indeed, FGM type-3 having the thickest ceramic top layer, presents deeper and more open cracks compared to FGM type-1 and 2. Finally, all the FGM present relatively good resistance in the tested conditions, but their behavior must however be confirmed by tests in an environment closer to reality.

3.3. Resistance of the FGM in the flame of a combustion chamber

The four types of FGM have been submitted to combustion tests in an H_2/O_2 flame to test their resistance in near real environmental conditions. The results obtained are very promising because after all the tests described in the experimental section, none of the tested FGM present visible severe degradation signs. FGM after tests I and IV are shown in Figure 9. Blue and green oxides are detectable on samples III-4 and IV-4 but are related to side effects. The stains, which are observable on some FGM have been identified as external pollution through EDS analysis as they are constituted of metallic elements (Fe, Al, Cr, Cu), which are coming from the degradation of the combustion chamber itself.

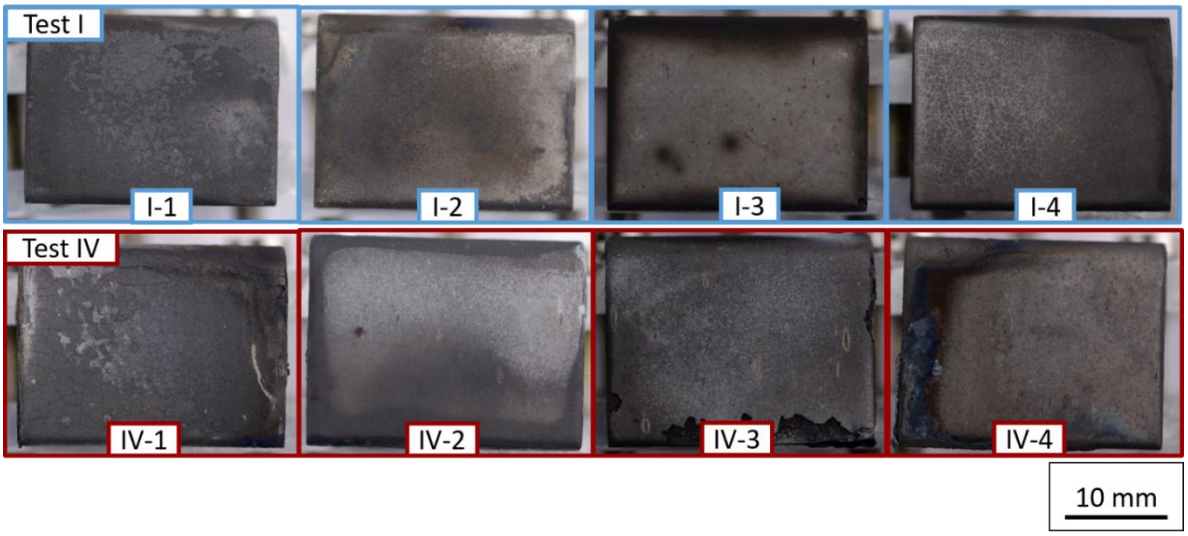

Figure 9 : Photographs of the surface of FGM after tests I and IV described in the experimental section.

The characterisation protocol followed after combustion tests is identical to the one after laser tests. Thus, SEM analyses of the surface have been first carried out. By contrast with the surface of FGM after laser tests, no crack network evolution is noticed after the combustion tests. Also, new cracks are not detectable on the surface, which means that the initial crack network, created during the high temperature thermal treatment, was stable under these conditions. Thus, this crack network probably allowed accommodating stresses during the different hot runs. Indeed, the cracks can close during heating and re open during the cooling phase of a hot run. In addition, XRD analyses of the surface of all FGM have been performed to study the phase composition. A typical example of an XRD analysis is presented in Figure 10. The orange line corresponds to the experimental diagram and the blue line to the calculated one. The green line represents the difference between experimental and calculated intensities. Also, the Rwp (weighted profile residue) is well below 10, which demonstrates the accuracy of the analysis.

DOI: 10.13009/EUCASS2023-295

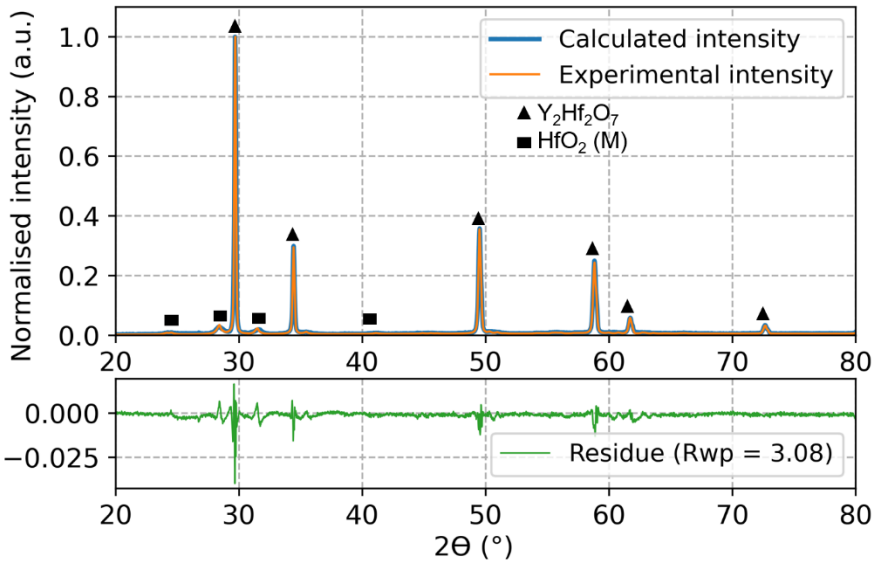

Figure 10 : XRD pattern and identification of the phases of sample I-4 after the test.

The main difference compared to the laser tests is that phase destabilisation at the surface of the FGM is not detectable in none of them. This is consistent with the fact that the atmosphere of the combustion test contains oxygen, which contributes to stabilise the $Y_2Hf_2O_7$, at the contrary to the vacuum atmosphere of the laser test. However, the presence of monoclinic HfO_2 (called HfO_2 (M)) is detected on some FGM, which was not previously observed. The presence of HfO_2 (M) is most probably related to the oxidation of HfC under these conditions. Indeed, after the last step of the elaboration process, which is the high temperature thermal treatment, HfC was detected through XRD analyses on the surface of some FGM. As combustion tests are performed in an oxidising atmosphere, HfC easily oxidises in HfO_2 (M). Thus, XRD diagrams can be simulated with $Y_2Hf_2O_7$, cubic HfO_2 (called HfO_2 (C)) and HfO_2 (M). Semi quantitative analyses of the surface phase composition are performed with the Direct Derivative Quant Method, which is an option in the HighScore Plus software. The quantifications are presented in Table 2. From this table, it is established that for FGM type-2,3,4, the fluorite phase $Y_2Hf_2O_7$ is the main phase detected, as expected from our previous studies [22,27,28]. For the FGM type-1, containing 12YSHf as a ceramic, the main phase is constituted of homogeneous cubic yttria enriched HfO_2 since Y_2O_3 has been introduced in lower amount (12 mol%). Indeed, the fluorite $Y_2Hf_2O_7$ phase is only formed above 33 mol% of Y_2O_3 in HfO_2. In addition, it can be seen from Table 2 that HfO_2 (M) is not detected on FGM type-2,3,4 after test IV. Thus, the formation of the fluorite $Y_2Hf_2O_7$ phase is promoted by the cumulative duration of hot runs in test IV, which is the longest one (1500 s).

Table 2 : Quantifications of the phases detected on the surface of FGM after tests.

Test number	**I**				**II**				**III**				**IV**			
Sample	I 1	I 2	I 3	I 4	II 1	II 2	II 3	II 4	III 1	III 2	III 3	III 4	IV 1	IV 2	IV 3	IV 4
HfO_2 (M) (wt%)	12.5	13	0	19	32.5	33	0	36	0	10	23	8	21.5	0	0	0
HfO_2 (C) (wt%)	87.5	0	0	0	67.5	0	0	0	100	0	0	0	78.5	0	8	0
$Y_2Hf_2O_7$ (C) (wt%)	0	87	100	81	0	67	100	64	0	90	77	92	0	100	92	100

SEM cross-section observations of FGM after the tests show neither oxidation nor total spallation of the samples. However, some local degradation signs are detectable, such as deflected cracks and partial spallation. Indeed, no additional cracks are created during the combustion tests, however, cracks propagate in depth and some of them are deviated. These deviations occur either at the ceramic/gradient interface or in the gradient layers, as shown in Figure 11(a). In addition, partial spallation is detectable on some samples, but is localised in pure ceramic layer only as it is visible in Figure 11(b). These local degradation signs are not damageable for the structure but could have become more concerning for longer tests.

DOI: 10.13009/EUCASS2023-295

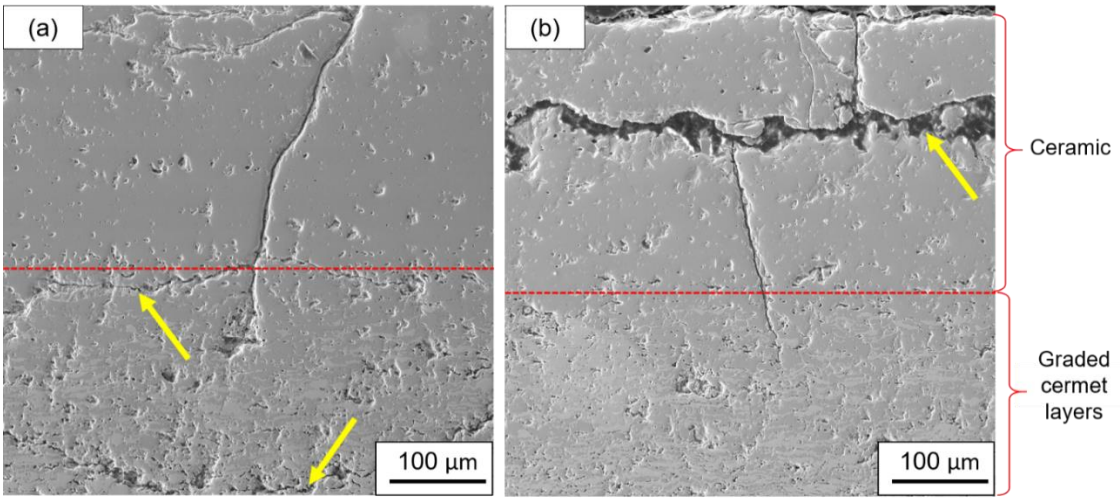

Figure 11 : SEM (SE) observations of the polished cross-sections of samples after tests (a) IV-3 and (b) IV-4 showing localised degradation phenomenon (yellow arrows) such as partial spallation and deflected cracks at ceramic/gradient interface or in the gradient.

Finally, panoramic optical cross section micrographs of the FGM (Figure 12) allow the determination of the linear density of cracks as a function of the test conditions (Figure 13). From this figure, it is clearly visible that the FGM types-3 and 4, which are composed of the thickest ceramic top layer have a lower linear density of cracks than FGM types-1 and 2. This is correlated to the fact that the crack depth is higher for FGM types-3 and 4, thus the volume of the non-stressed plastic zone around the crack is more important. As it is impossible to create new cracks in this plastic zone, the distance between cracks becomes larger. However, increasing the density of cracks promotes a better resistance to thermal shocks in the FGM. Indeed, Han et al. [29] demonstrated through simulations that multiple cracking in TiC/Ni FGM is beneficial for thermal shock resistance because it reduces the stresses in the material. Considering this, the authors explain that the worse scenario is the presence of a single crack in the FGM. This corroborates with the study of Kokini et al. [14], who found that both multiple cracking associated to a progressive evolution of the chemical composition in the FGM provides a better resistance to thermal shock.

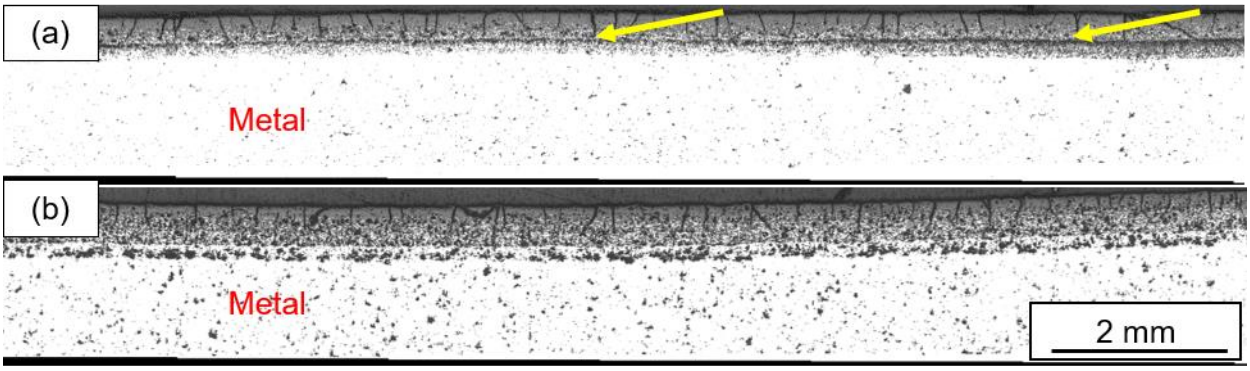

Figure 12: Optical micrographs of the cross-sections of FGM (a) IV-1 and (b) IV-2 in which yellow arrows correspond to the porosity rearrangement inside the gradient layers (dark part of the FGM is ceramic and white part is metal).

DOI: 10.13009/EUCASS2023-295

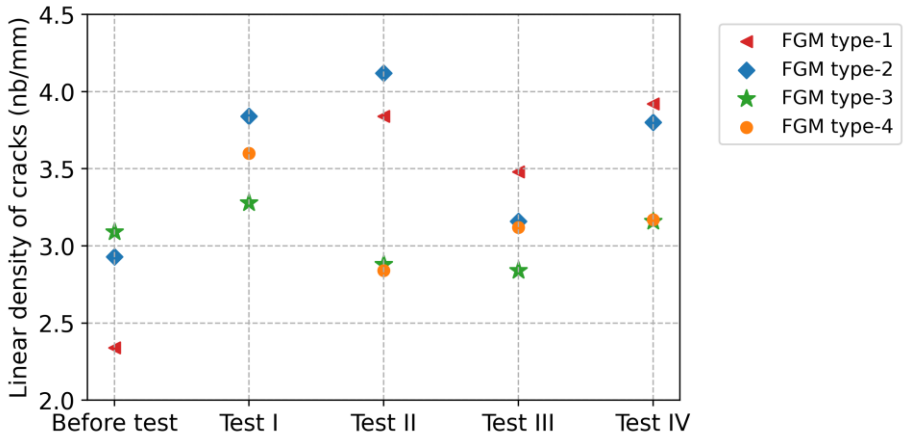

Figure 13 : Linear density of cracks in longitudinal cross section of FGM as a function of the test conditions.

Optical micrographs also reveal that for type-1 FGM, a reorganisation of porosity inside the gradient occurs. Indeed, the porosities are reorganised in a way to join each other. Thus, a horizontal line of porosities appears inside the gradient layers of type-1 FGM, as shown by the yellow arrows in Figure 12(a). With a longer time exposure to the flame, this rearrangement could have led to possible spallation, which would have been detrimental for the structure, especially inside the gradient layer. As this phenomenon is only observed for type-1 FGM, it is probably related to the ceramic composition. Two hypothesis can explain this phenomenon. First, increasing the amount of Y_2O_3 in HfO_2 may imply a better resistance to sintering, occurring during the combustion tests. Thus, for FGM type-1 containing only 12 mol% of Y_2O_3, the sintering behavior between ceramic grains and between metal particles might be highly different. Indeed, Bahr et al. [30] studied the sequence of damages occurring in a graded thermal barrier coating. They found that two effects contribute to damages during cyclic heating, which are the sintering and the high temperature creep. Both of them are responsible for shrinkage of the ceramic part, which finally leads to spallation. Another explanation is the thermal expansion mismatch between the ceramic and metal particles. Indeed, the thermal expansion coefficients of 12YSHf and 33YSHf were determined up to 1673 K in our previous studies and are respectively 11.48 x 10^{-6} K^{-1} and 10.72 x 10^{-6} K^{-1} [27,28]. As the thermal expansion coefficient of the metal is well below 10, the thermal expansion mismatch between the metal and the ceramic is higher for the 12YSHf ceramic compared to the 33YSHf ceramic. This superior mismatch can lead to higher stresses between ceramic and metal particles in the graded part, leading to partial decohesion or porosity coalescence.
Considering all these data, the most interesting type of FGM to withstand hot tests in a combustion chamber seems to be the type-2 FGM, combining a thin ceramic top layer composed of 33YSHf.

4. Conclusion

The influence of the composition profile of ceramic/metal FGM on the thermomechanical resistance in specific atmospheres was determined. More specifically, four types of FGM, which differ in the nature of the ceramic, the thickness of the pure ceramic layer and the graded layers, have been manufactured through APS and submitted to a high temperature densification thermal treatment. After that, FGM types-1, 2, 3 were tested on a laser test bench and FGM types-1, 2, 3, 4 were tested in the flame of a combustion chamber. The laser tests allow to determine the resistance of such FGM submitted to thermal shock (200 K s^{-1}) under vacuum for various temperature differences, up to 2623 K. The combustion tests allow to qualify the FGM resistance in a combustion flame (3200 K) in near real environmental conditions, as the flame combustion products are mainly constituted of water vapor. The main conclusions are the followings.
First, the nature of the ceramic influences the behavior of FGM submitted to laser tests. Indeed, for 33YSHf ceramics, a phase destabilisation occurs at the surface, for temperatures above 2143 K. This destabilisation is associated to a crack network evolution before and after the laser test, which may be attributed to diffusion sintering linked phenomena. After laser tests, none of the FGM present spallation of the ceramic layer even if the higher the number of cycles, the greater the depth of the crack. These tests allow to qualify the resistance of FGM submitted to thermal shock but are far from real environmental conditions. Thus, FGM have been submitted to a combustion H_2/O_2 flame. After combustion tests, none of the FGM present complete spallation nor oxidation, which means that the ceramic top layer successfully acts as a thermal and environmental barrier coating. However, some local degradation signs appeared such as local spallation or deflected cracks. Furthermore, the thickness of the ceramic top layer seems to have a decisive role on the density and depth of cracks. The most favorable case seems to be for the thinnest ceramic top layer.

DOI: 10.13009/EUCASS2023-295

Combining all these data, it seems that under near real conditions, a thin ceramic top layer composed of 33YSHf is more valuable for the FGM resistance.
To pursue this study, oxidation tests under water vapor with laser thermal flux will be carried out. The surface temperature is known with precision under these test conditions, which allows to asset the link between the temperature and the degradation phenomena related to oxidation. Moreover, the testing conditions may be pushed forward to determine the temperature limit of use under water vapor.

Acknowledgments

The authors would like to thank Thibaut ARCHER and Damien BAUTISTA for their help with the laser test bench and Quentin BARRES for EDS analysis.

References

[1] Agreement of the member state committee on the identification of hydrzazine as a substance of very high concern, Eur. Chem. Agency. (2011).
[2] M. Negri, Replacement of Hydrazine: Overview and First Results of the H2020 Project Rheform, (2015).
[3] R. Amrousse, T. Katsumi, N. Azuma, K. Hori, Hydroxylammonium nitrate (HAN)-based green propellant as alternative energy resource for potential hydrazine substitution: From lab scale to pilot plant scale-up, Combust. Flame. 176 (2017) 334–348. https://doi.org/10.1016/j.combustflame.2016.11.011.
[4] J. Wallbank, P. Sermon, A. Baker, L. Courtney, R. Sambrook, Nitrous oxide as a green monopropellant for small satellites., Proc. 2nd Int. Conf. Green Propellants Space Propuls. Sard. Italy. (2004) 7–8.
[5] A. Kawasaki, R. Watanabe, Thermal fracture behavior of metal/ceramic functionally graded materials, Eng. Fract. Mech. 69 (2002) 1713–1728. https://doi.org/10.1016/S0013-7944(02)00054-1.
[6] N. Cherradi, A. Kawasaki, M. Gasik, Worldwide trends in functional gradient materials research and development, Compos. Eng. 4 (1994) 883–894. https://doi.org/10.1016/S0961-9526(09)80012-9.
[7] H.-P. Xiong, A. Kawasaki, Y.-S. Kang, R. Watanabe, Experimental study on heat insulation performance of functionally graded metal/ceramic coatings and their fracture behavior at high surface temperatures, Coat. Technol. 194 (2005) 203–214. https://doi.org/10.1016/j.surfcoat.2004.07.069.
[8] M. Anaz Khan, A. Vivek Anand, M. Duraiselvam, K. Srinivas Rao, R. Arvind Singh, S. Jayalakshmi, Thermal Shock Resistance and Thermal Insulation Capability of Laser-Glazed Functionally Graded Lanthanum Magnesium Hexaluminate/Yttria-Stabilised Zirconia Thermal Barrier Coating, Materials. 14 (2021) 3865. https://doi.org/10.3390/ma14143865.
[9] Z. Gan, H.W. Ng, Experiments and inelastic finite element analyses of plasma sprayed graded coatings under cyclic thermal shock, Mater. Sci. Eng. A. 385 (2004) 314–324. https://doi.org/10.1016/j.msea.2004.06.053.
[10] A. Kawasaki, R. Watanabe, Evaluation of thermomechanical performance for thermal barrier type of sintered functionally graded materials, Compos. Part B Eng. 28 (1997) 29–35. https://doi.org/10.1016/S1359-8368(96)00017-0.
[11] S. Nath, I. Manna, J.D. Majumdar, Kinetics and mechanism of isothermal oxidation of compositionally graded yttria stabilized zirconia (YSZ) based thermal barrier coating, Corros. Sci. 88 (2014) 10–22. https://doi.org/10.1016/j.corsci.2014.06.050.
[12] K.A. Khor, Y.W. Gu, Thermal properties of plasma-sprayed functionally graded thermal barrier coatings, Thin Solid Films. 372 (2000) 104–113. https://doi.org/10.1016/S0040-6090(00)01024-5.
[13] K.A. Khor, Z.L. Dong, Y.W. Gu, Influence of oxide mixtures on mechanical properties of plasma sprayed functionally graded coating, Thin Solid Films. 368 (2000) 86–92.
[14] K. Kokini, J. DeJonge, S. Rangaraj, B. Beardsley, Thermal shock of functionally graded thermal barrier coatings with similar thermal resistance, Surf. Coat. Technol. 154 (2002) 223–231. https://doi.org/10.1016/S0257-8972(02)00031-2.
[15] Z.L. Dong, K.A. Khor, Y.W. Gu, Microstructure formation in plasma-sprayed functionally graded NiCoCrAlY/yttria-stabilized zirconia coatings, Surf. Coat. Technol. 114 (1999) 181–186. https://doi.org/10.1016/S0257-8972(99)00049-3.
[16] N. Nayebpashaee, S.H. Seyedein, M.R. Aboutalebi, H. Sarpoolaky, M.M. Hadavi, Simulation of the Effect of Sub-Micron Interface Roughness on the Stress Distribution in Functionally Graded Thermal Barrier Coatings, Adv. Ceram. Prog. 1 (2015) 40–47. https://doi.org/10.30501/ACP.2015.69999.
[17] Y. Sohda, Carbon/carbon composites coated with SiC/C functionally gradient com- positions, Ceram. Trans. 125 (1993) 34.
[18] M. Suzuki, M. Shahien, K. Shinoda, J. Akedo, The Current Status of Environmental Barrier Coatings and Future Direction of Thermal Spray Process, Mater. Trans. 63 (2022) 1101–1111. https://doi.org/10.2320/matertrans.MT-T2021003.

DOI: 10.13009/EUCASS2023-295

[19] J. Wang, H.P. Li, R. Stevens, Hafnia and hafnia-toughened ceramics, J. Mater. Sci. 27 (1992) 5397–5430. https://doi.org/10.1007/BF00541601.
[20] D. Zhu, N.P. Bansal, R.A. Miller, Thermal Conductivity and Stability of HfO_2 $-Y_2O_3$ and $La_2Zr_2O_7$ Evaluated for 1650°C Thermal/Environmental Barrier Coating Applications, 105th Annu. Meet. Expo. Am. Ceram. Soc. Spons. Am. Ceram. Soc. (2003) 329–343. https://doi.org/10.1002/9781118406892.ch23.
[21] S. Sampath, H. Herman, N. Shimoda, T. Saito, Thermal Spray Processing of FGMs, MRS Bull. 20 (1995) 27–31.
[22] L. Audouard, M.G. Tsoutsouva, N. Horezan, E. Rimpot, J.F. Justin, P. Bertrand, C. Langlade, M. Garcia, A. Julian-Jankowiak, Chemical and microstructural characterisation of HfO_2-Y_2O_3 ceramics with high amount of Y2O3 (33, 40 and 50 mol. %) manufactured using spark plasma sintering, J. Eur. Ceram. Soc. 43 (2023) 2093–2103. https://doi.org/10.1016/j.jeurceramsoc.2022.12.061.
[23] J. Zhao, Y. Zhang, H. Gong, Y. Zhang, X. Wang, X. Guo, Y. Zhao, Fabrication of high-performance Y_2O_3 stabilized hafnium dioxide refractories, Ceram. Int. 41 (2015) 5232–5238. https://doi.org/10.1016/j.ceramint.2015.01.047.
[24] Y. Liu, H. Yin, Y. Tang, Y. Xin, H. Yuan, X. Ren, Q. Wan, Synthesis mechanism and properties of lightweight mullite-corundum refractories obtained through high temperature liquid-assisted micrometer-scale Kirkendall effect, Ceram. Int. 47 (2021) 9234–9244. https://doi.org/10.1016/j.ceramint.2020.12.049.
[25] S. Gopalan, A.V. Virkar, Interdiffusion and Kirkendall Effect in Doped $BaTiO_3$-$BaZrO_3$ Perovskites: Effect of Vacancy Supersaturation, J. Am. Ceram. Soc. 82 (2004) 2887–2899. https://doi.org/10.1111/j.1151-2916.1999.tb02173.x.
[26] L.G. Feinstein, J.B. Bindell, The failure of aged Cu-Au thin films by Kirkendall porosity, Thin Solid Films. 62 (1979) 37–47. https://doi.org/10.1016/0040-6090(79)90379-1.
[27] L. Sévin, V. Razafindramanana, A. Julian-Jankowiak, J.-F. Justin, F. Mauvy, F. Rebillat, Effect of high-content Yttria on the thermal expansion behaviour and ionic conductivity of a stabilised cubic Hafnia, J. Eur. Ceram. Soc. 40 (2020) 5859–5869. https://doi.org/10.1016/j.jeurceramsoc.2020.05.044.
[28] L. Sévin, L. Audouard, V. Razafindramanana, F. Mauvy, L. Galzin, J.-F. Justin, P. Bertrand, C. Langlade, M. Garcia, A. Julian-Jankowiak, Phase stabilisation, thermal expansion and ionic conductivity of high content rare earth oxide (Lu_2O_3, Y_2O_3 and Gd_2O_3) stabilised cubic hafnia, J. Eur. Ceram. Soc. 43 (2023) 4153–4166. https://doi.org/10.1016/j.jeurceramsoc.2023.03.006.
[29] J.-C. Han, B.-L. Wang, Thermal shock resistance enhancement of functionally graded materials by multiple cracking, Acta Mater. 54 (2006) 963–973. https://doi.org/10.1016/j.actamat.2005.10.036.
[30] H.-A. Bahr, H. Balke, T. Fett, I. Hofinger, G. Kirchhoff, D. Munz, A. Neubrand, A.S. Semenov, H.-J. Weiss, Y.Y. Yang, Cracks in functionally graded materials, Mater. Sci. Eng. A. 362 (2003) 2–16. https://doi.org/10.1016/S0921-5093(03)00582-3.